

# Design, Modal and Stress Analysis of Aircraft Composite Wing

Joyel K Joseph

M. Tech. Machine design  
T.John Institute of Technology  
Bangalore

Avinash Babu

Asst. Professor, Dept. of Mechanical.  
T.John Institute of Technology  
Bangalore

**Abstract**— This paper deals with the Design, modal and static stress analysis of composite wing structure for a transport aircraft. The aim is to design and analyze the Skin stringers, longerons and frames of a transport aircraft for the stresses and displacements due to the applied loads. It deals with the comparative study on particular transport aircraft. The optimum design parameters for a transport aircraft are suitably selected based on the fuselage and wing modal was design using the CATIA-V5 R19 software, which is developed by Dassault systems and is very famous for its 3D modeling capabilities. The major Wing design parameters were explained in detail and its configuration has been described. Different types of loads acting on the wings are determined and the moments, displacements, etc., are also determined. The wing structure was also explained and functions of each component and their arrangement are also studied. The methodology of finite element method and the detailed description about various FEM tools have been studied and implemented in this work. The procedure of finite element method was followed to analyze the model. The analyzing part of this project is done using the NASTRAN-PATRAN package and the results were discussed

**Keywords**— Composite, CATIA-V5 R19 , MSC NASTRA, MSC PATRAN, FEM.

## I. INTRODUCTION

As a kind of new material, the advanced composite material brings about great revolution to the aircraft industry since it was introduced in the 1960s. With its wide application in aerospace structure, the advanced composite material is named as “the four main materials of aerospace

Structure” along with aluminium alloy, titanium alloy, and alloy steel. The advanced composite material has its own prominent features, such as high specific strength, high specific modulus, designable performance and integral forming easily, etc. With the application of the advanced composites, the weight of the aircraft structure can be reduced by about 25% ~ 30% compared to the conventional metal structures. Moreover, the aerodynamic and flight performances can be

Improved to the levels that the conventional materials can hardly achieve. The extensive application of advanced composites is also able to promote some further technology development of structure stealth and intelligent structure design. The aircraft structure performance is significantly dependent on the part and quality of the advanced composites used in aircraft. However, it is difficult to achieve good designs of the composites in aircraft structure to guarantee

requirements for different missions. Therefore, to fully explore the directional properties of composites, the designable ability of structure performance and the excellent manufacturability of large component integral forming, it is necessary to introduce the principle of optimization to the composite structure design [1-6]. By using parametric modelling technique, the parametric finite element model is established to conduct stress and strain analysis of the wing. Given any set of geometric parameters, the geometric modelling, meshing, strain and stress analysis can be automatically carried out in sequence. To ensure the optimal solution can be obtained, a two-step optimization search strategy which combines genetic algorithm (GA) and sequential quadratic programming (SQP) is proposed during optimization. It is concluded that this two-step optimization search strategy can greatly enhance the efficiency of finding the true optimal solution through comparing this method with GA.

## II. GEOMETRICAL CONFIGURATION

The wing design is an iterative process and the selections or calculations are usually repeated several times. A variety of tools and software based on aerodynamics and numerical methods have been developed in the past decades, there by a reduction in the number of iterations is observed. Normally two spar construction is common in transport aircraft wing design. The spar near to the leading edge of the wing is called as front spar and the spar closer to the aft portion of the wing is called as rear spar of the wing. One end of the spar near the root of the wing is connected to the fuselage called root of wing, the other end towards the tip of the wing is a free end. This configuration is very similar to the cantilever beam arrangement in any engineering structure. Spars and Ribs are connected using L angle fittings. The following equations are used in design of wing. Figure 1 below shows the dimensions of wing Figure 2 shows the complete wing structure modelled in CATIA V5.

### A. Lift coefficient

$$C_{Lmax} = 2 \times W / \rho \times (V_{STALL})^2 \times S \quad (1)$$

$C_{Lmax}$  =Coefficient of lift

W =Maximum take off weight

$V_{STALL}$  =Cruise speed x0.25

S =Wing area

$\rho$  =Density

B. Chord length

$$C = S/b \quad (2)$$

C = Chord length

S = Wing area

b = Wing span

C. Induced drag coefficient

$$C_{Di} = C_L^2 / (\pi \times e \times AR) \quad (3)$$

e = Oswald efficiency factor

AR = Aspect Ratio

D. Oswald efficiency factor

$$e = 4.61(1 - 0.045A^{0.68})(\cos(A_{LE}))^{0.15-3.1} \quad (4)$$

$A_{LE}$  =sweep back angle

E. Profile drag coefficient

$$C_{Do} = C_{fe} \times (S_{wef} / S_{ref}) \quad (5)$$

$C_{fe}$  = Equivalent skin friction co efficient

$S_{wef} / S_{ref}$  = Wetted area ratios

F. Total drag coefficient

$$C_D = C_{Do} + C_{Di} \quad (6)$$

$C_{Di}$  = Induced drag co efficient

$C_{Do}$  = Profile drag co efficient

G. Root chord

$$C_{root} = 2 \times S / b \times (1 + \lambda) \quad (7)$$

$\lambda$  = Taper ratio

H. Tip chord

$$C_{tip} = \lambda \times C_{root} \quad (8)$$

$C_{tip}$  = Tip chord

$C_{root}$  = Root chord

I. Exposed wing span

$$Semispan = b/2 \quad (9)$$

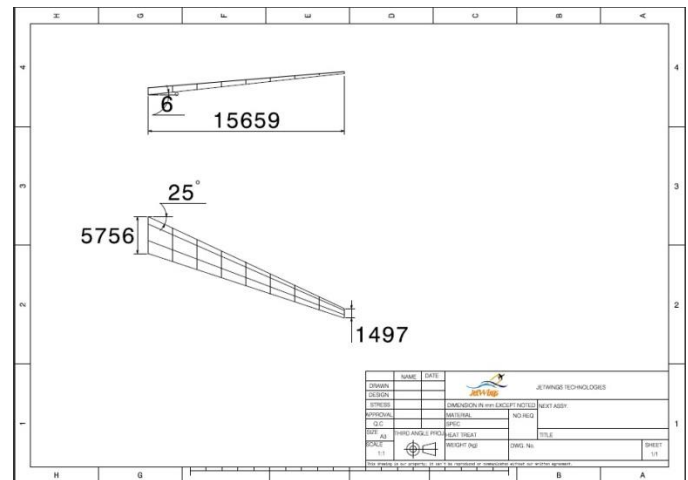


Fig.1 Dimensions of wing.

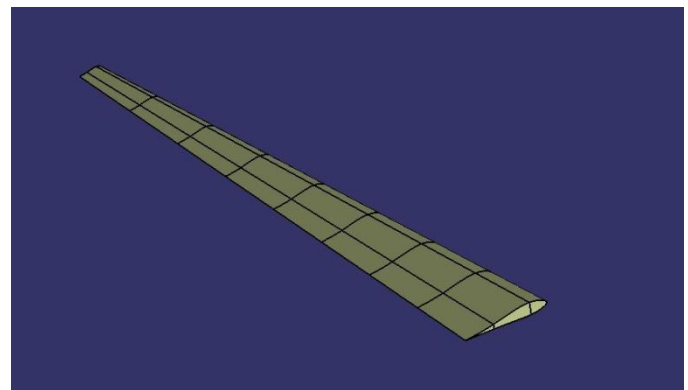


Fig.2 Wing structure modeled using CATIA V5.

### III.MATERIAL SELECTION AND SPECIFICATION

The general principle of fibre reinforced plastic consists of the synergetic effect when combining the excellent mechanical properties of thin, application tailored filaments with a supporting matrix material.

The first large-scale applications of FRP in aircraft wing design date back to the 1960s, while the development of composite modelling and optimization methods essentially started in the 1970s aircraft manufacturers like Airbus and Boeing with the A350 and B787 have just lately introduced aircraft types featuring entire components like wing and fuselage made of composites

Fiber reinforced plastics (FRP) represented one of the most important milestones in the latest aviation history. A prominent advantage of composites over metal-based materials is found in the excellent stiffness to mass and strength to mass ratios that go along with the considerably lower material density.

TABLE 1. Mechanical Properties of the Carbon-Fiber-Reinforced Plastic

Property	Method of testing	No. of samples	Average value, $\text{kgf} \cdot \text{cm}^{-2}$	Mean square deviation, $\text{kgf} \cdot \text{cm}^{-2}$	Coefficient of variation, %
Modulus of elasticity, $E_\varphi$	Bending of the ring by concentrated forces	9	$14 \cdot 10^5$	$5,05 \cdot 10^5$	36,0
Modulus of elasticity, $E_T$	Compression of a cylindrical sample	8	$0,82 \cdot 10^5$	$0,23 \cdot 10^5$	28,1
Modulus of interlayer shear, $G_{\varphi T}$	Torsion of the ring (see [4])	6	$0,31 \cdot 10^5$	$0,03 \cdot 10^5$	9,3
Strength in a peripheral direction, $\sigma_{\varphi, B}$	Stretching of the ring using the semidisk method	19	4676,2	932,1	19,8
Strength with respect to interlayer tearing apart, $\sigma_{T, B}$	Bending of a sectioned ring (see [5])	6	143,3	14,2	9,9
Strength with respect to interlayer shear, $\tau_{\varphi, B}$	Bending of a segment of the ring	14	247,5	33,1	13,4

Table I. Mechanical properties of the carbon fiber reinforced plastic

#### IV. FINITE ELEMENT MODELING OF WING STRUCTURE

The model assembly is converted to igs file and imported to MSC PATRAN as shown in fig 3:

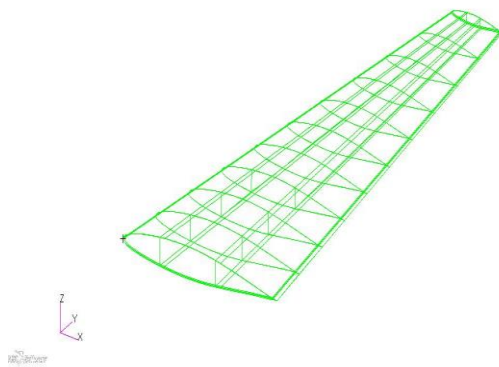


Fig.3 Model imported to MSC PATRAN

Finite element modelling is completed in MSc Patran using the IGS file as geometry, the element type used for meshing was 2D shell elements with QUAD4 element topology and different parts are connected using RBE2 connection as shown in the following figures.

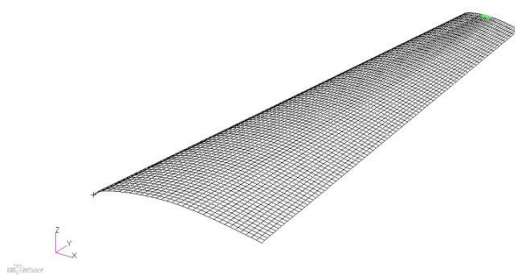


Fig.4 Upper skin meshed.

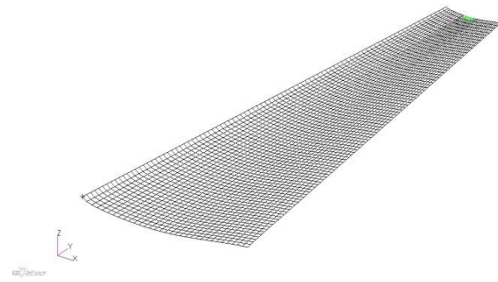


Fig.5 Lower skin meshed.

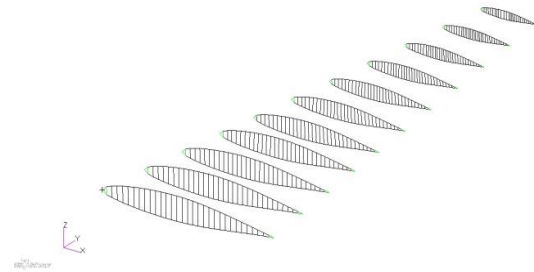


Fig.6 Ribs meshed.

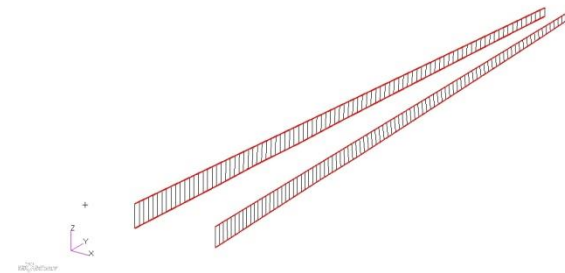


Fig.7 Spars meshed.

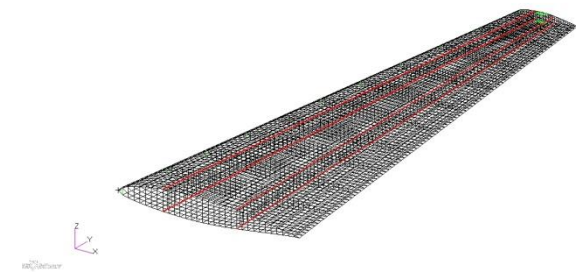


Fig.8 Complete meshed wing.

#### V. LOAD AND BOUNDARY CONDITIONS

Verification for the boundary, duplicates is carried out. Normal for each element is assigned. The material properties are assigned to every element in the model. The stress analysis of the wing structure is carried out using the finite element analysis approach.

The wing structure of an aircraft is connected to the fuselage through keel beam. So the wing structure is act as a cantilever beam connected with fuselage. One end of the wing structure can be fixed and taken as the boundary conditions of the model. This was satisfied by fixing all six degrees of freedom on the nodes corresponding to the fixing point.

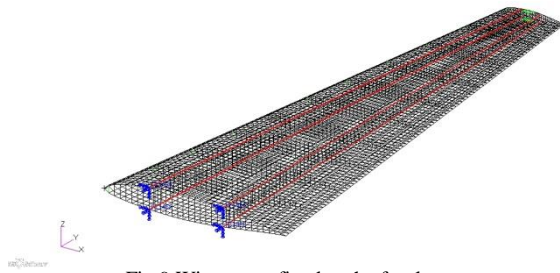


Fig.9 Wing spars fixed to the fuselage.

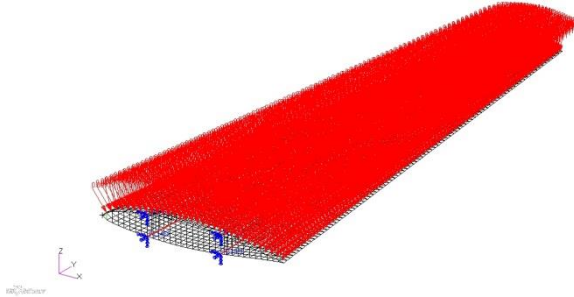


Fig.10 Pressure acting on the skin of wing.

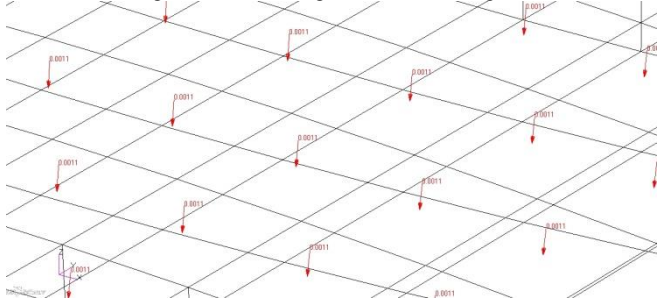


Fig.11 Pressure forces acting on the elementary areas.

## VI. FE MODELING AND STRESS ANALYSIS OF WING STRUCTURE

The static analyses were conducted by using the solver 101 module of MSC®/ NASTRAN package program. Figures shows the displacement field of the wing torque box under the load conditions. Figures also shows the stress distribution on the internal structure and the maximum stress location respectively. Comparing this value with the yield strength of Aluminium 7075-T651, which was given as 503 [MPa], it was concluded that the wing is far safe with a large margin of safety

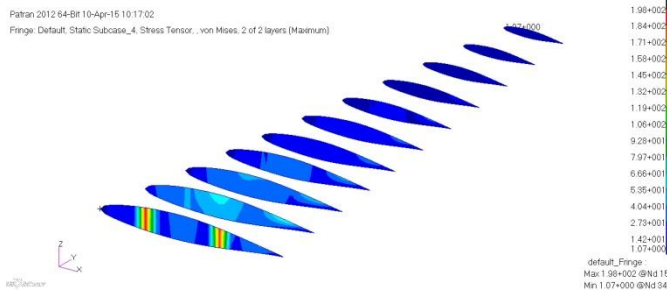


Fig.12 Ribs of aluminium alloy.

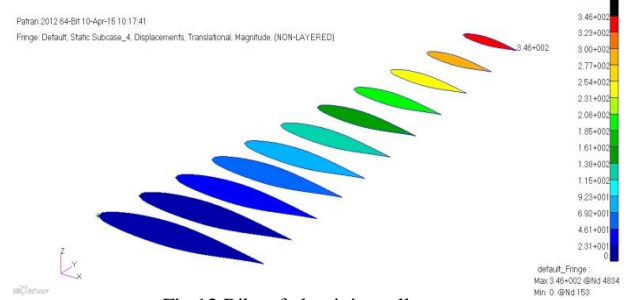


Fig.13 Ribs of aluminium alloy.

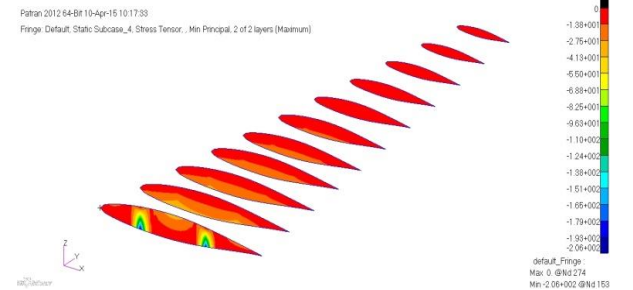


Fig.14 Ribs of aluminium alloy.

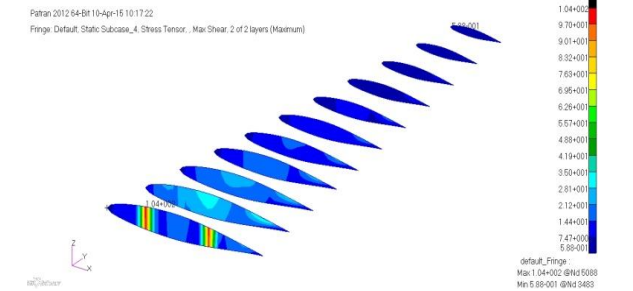


Fig.15 Ribs of aluminium alloy.

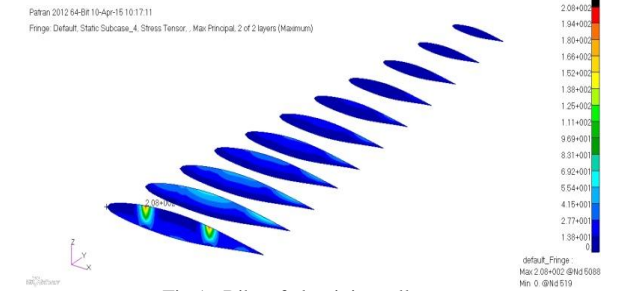


Fig.16 Ribs of aluminium alloy.

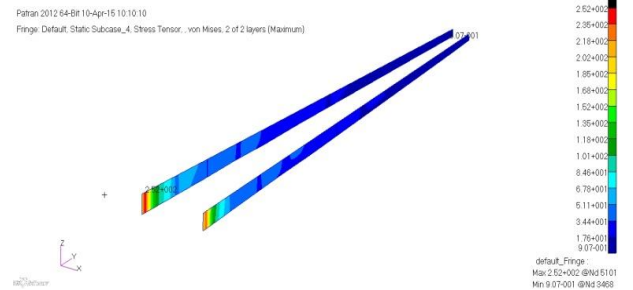


Fig.17 Spars of aluminium alloy.



Patran 2012 64-Bit 10-Apr-15 10:10:45  
Fringe: Default: Static Subcase\_4, Stress Tensor, Max Principal, 2 of 2 layers (Maximum)

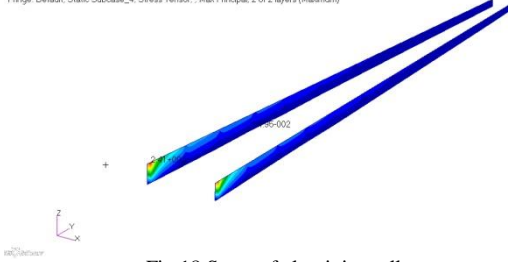


Fig.18 Spars of aluminium alloy.

Patran 2012 64-Bit 10-Apr-15 10:10:52  
Fringe: Default: Static Subcase\_4, Stress Tensor, Min Principal, 2 of 2 layers (Maximum)

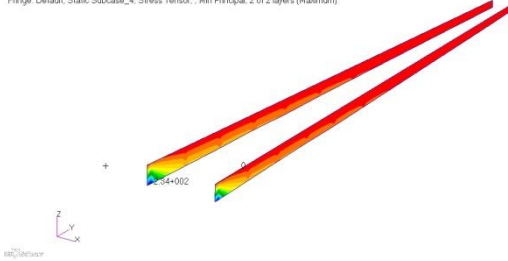


Fig.19 Spars of aluminium alloy

Patran 2012 64-Bit 10-Apr-15 10:11:01  
Fringe: Default: Static Subcase\_4, Stress Tensor, Max Shear, 2 of 2 layers (Maximum)

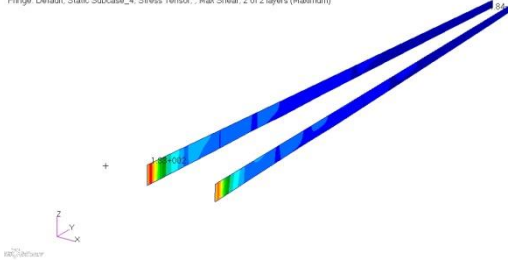


Fig.20 Spars of aluminium alloy.

Patran 2012 64-Bit 10-Apr-15 10:11:01  
Fringe: Default: Static Subcase\_4, Stress Tensor, Max Shear, 2 of 2 layers (Maximum)

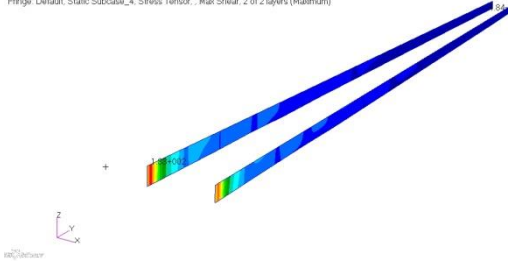


Fig.21 Spars of aluminium alloy.

Patran 2012 64-Bit 10-Apr-15 10:11:13  
Fringe: Default: Static Subcase\_4, Displacements, Translational, Magnitude (NON-LAYERED)

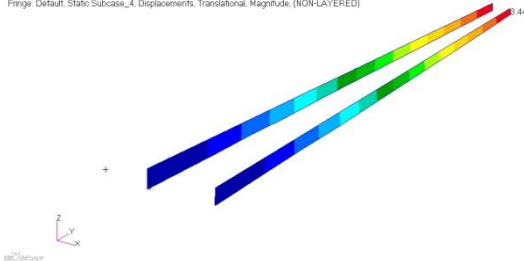


Fig.22 Spars of aluminium alloy.

Patran 2012 64-Bit 10-Apr-15 10:13:54  
Fringe: Default: Static Subcase\_5, Stress Tensor, von Mises, 6 of 6 layers (Maximum)

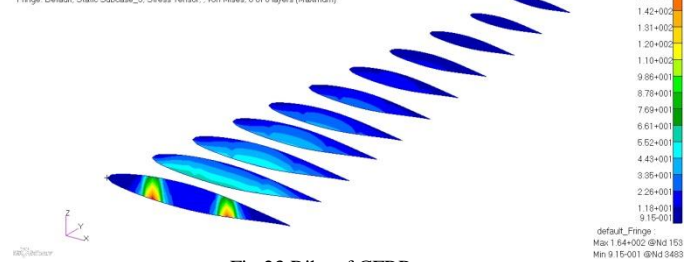


Fig.23 Ribs of CFRP.

Patran 2012 64-Bit 10-Apr-15 10:14:24  
Fringe: Default: Static Subcase\_5, Stress Tensor, Max Principal, 6 of 6 layers (Maximum)

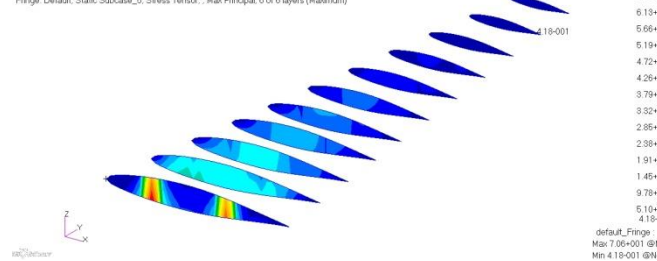


Fig.24 Ribs of CFRP.

Patran 2012 64-Bit 10-Apr-15 10:14:33  
Fringe: Default: Static Subcase\_5, Stress Tensor, Min Principal, 6 of 6 layers (Maximum)

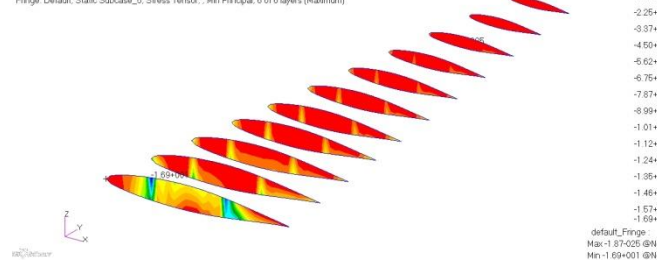


Fig.25 Ribs of CFRP.

Patran 2012 64-Bit 10-Apr-15 10:15:35  
Fringe: Default: Static Subcase\_5, Displacements, Translational, Magnitude (NON-LAYERED)

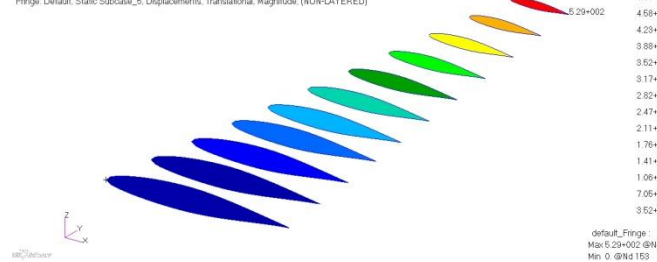


Fig.26 Ribs of CFRP.

Patran 2012 64-Bit 10-Apr-15 10:15:24  
Fringe: Default: Static Subcase\_5, Stress Tensor, Max Shear, 6 of 6 layers (Maximum)

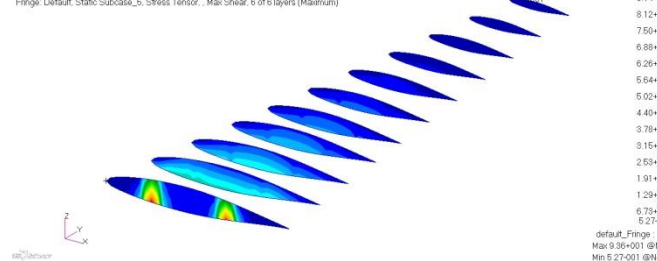


Fig.27 Ribs of CFRP.

Patran 2012 64-Bit 10-Apr-15 10:11:50  
Fringe: Default: Static Subcase\_5, Stress Tensor, Max Shear, 6 of 6 layers (Maximum)

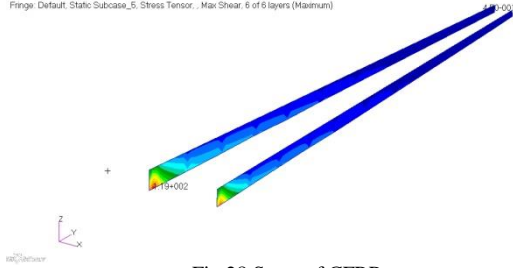


Fig.28 Spars of CFRP.

Patran 2012 64-Bit 10-Apr-15 10:12:08  
Fringe: Default: Static Subcase\_5, Stress Tensor, von Mises, 6 of 6 layers (Maximum)

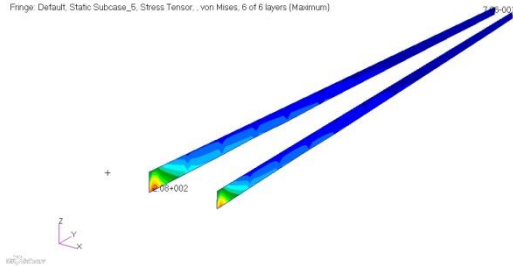


Fig.29 Spars of CFRP.

Patran 2012 64-Bit 10-Apr-15 10:12:16  
Fringe: Default: Static Subcase\_5, Stress Tensor, Max Principal, 6 of 6 layers (Maximum)

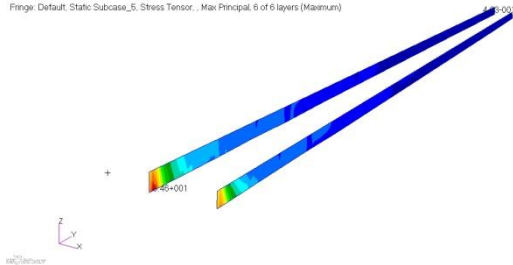


Fig.30 Spars of CFRP.

Patran 2012 64-Bit 10-Apr-15 10:12:24  
Fringe: Default: Static Subcase\_5, Stress Tensor, Min Principal, 6 of 6 layers (Maximum)

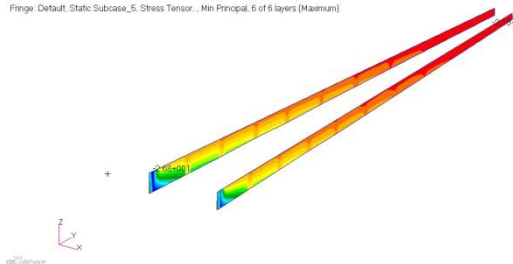


Fig.31 Spars of CFRP.

Patran 2012 64-Bit 10-Apr-15 10:12:32  
Fringe: Default: Static Subcase\_5, Displacements, Translational, Magnitude (NON-LAYERED)

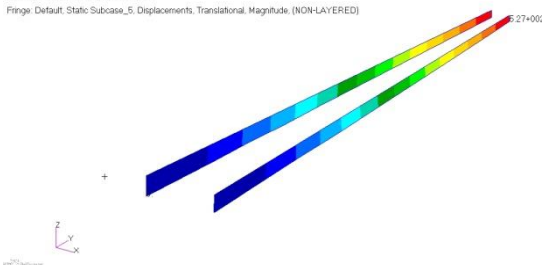


Fig.32 Spars of CFRP.

## VII. CONCLUSION

The Von – Mises stress distribution in the case of wing is less towards the wings leading and trailing edges and decreases towards the wing tip. The variation in fiber orientation at the same skin thickness will produce the variation in the Von Mises stress (increase or decrease). Maximum values of Von-Mises stress was observed at the support position of the combined wing. The largest magnitude of displacement was obtained at the free end of the combined wing. The replacement of Aluminium alloy by CFRP reduces the total weight of the aircraft wing by 23.7%. By comparing the stress and displacement in Table 2, it is concluded that the CFRP is seen to have better performance. Thus it is desirable to adopt the CFRP material for composite aircraft wings in comparison with the conventional aluminium alloy considered in the present study.

CFRP	obtained stress	uts	RF value	MOS
von mises	216	1450	6.712963	5.712963
max principal	90	1450	16.111111	15.111111
max shear	123	870	7.073171	6.073171
<b>Aluminium</b>				
von mises	252	483	1.916667	0.916667
max principal	241	483	2.004149	1.004149
max shear	130	283	2.176923	1.176923

Table II. RF table comparing the responses of CFRP and Aluminium alloy

## REFERENCES

- [1] International Journal of Innovative Research in Science, Engineering and Technology Vol. 2, Issue 6, June 2013. Jones R. T "The spanwise distribution of lift for minimum induced drag of wings having a given lift and a given bending moment" Tech. Rep. TN-2249, NASA, December 1950.
- [2] School of Aerospace Engineering, Beijing Institute of Technology, Beijing 100081, China. The Open Mechanical Engineering Journal, 2011, 5, 11-18.
- [3] Journal of Engineering and Development, Vol. 12, No. 1, March (2008)
- [4] Graeme J. Kennedy and Joaquim R. R. A. Martinsy, "A Comparison of Metallic and Composite Aircraft Wings Using Aerostructural Design Optimization", University of Toronto Institute for Aerospace Studies, Toronto, ON, Canada.
- [5] Peter J Rohl, Dimitri N Mavris and Daniel P Schrage, "Combined aero dynamic and Structural Optimization of a high speed civil transport Wing", School of Aerospace Engineering, Georgia Institute of Technology Atlanta.
- [6] Kong, h. park, y. Kim and k. Kang "Structural design on wing of a small scale wig vehicle with carbon/epoxy and foam sandwich composite structure", 16th international conference on composite material
- [7] F. H. Darwisha, G. M. Atmeh and Z. F. Hasan "Design analysis and modeling of general aviation aircraft", Jordan Journal of Mechanical and Industrial Engineering Volume 6, Number 2, pp 183-191, 2012.
- [8] Levent Ünluşoy "Structural design and analysis of the mission adaptive wings of an unmanned aerial vehicle", A thesis submitted to Middle East Technical University, February 2010.